

A Microliter Capillary Rheometer for Characterization of Protein Solutions

STEVEN D. HUDSON,¹ PRASAD SARANGAPANI,² JAI A. PATHAK,² KALMAN B. MIGLER¹¹Polymers and Complex Fluids Group, Materials Science and Engineering Division, National Institute of Standards and Technology, Gaithersburg, Maryland 20899²Formulation Sciences Dept., MedImmune, One MedImmune Way, Gaithersburg, Maryland 20878

Received 28 May 2014; revised 15 September 2014; accepted 17 September 2014

Published online 10 October 2014 in Wiley Online Library (wileyonlinelibrary.com). DOI 10.1002/jps.24201

ABSTRACT: Rheometry is an important characterization tool for therapeutic protein solutions because it determines syringeability and relates indirectly to solution stability and thermodynamic interactions. Despite the maturity of rheometry, there remains a need for a rheometer that meets the following three needs of the biopharmaceutical industry: small volume; large dynamic range of shear rates; and no air–sample interface. Here, we report the development of a miniaturized capillary rheometer that meets these needs and is potentially scalable to a multiwell format. These measurements consume only a few microliters of sample and have an uncertainty of a few percent. We demonstrate its performance on monoclonal antibody solutions at different concentrations and temperatures. The instrument has a dynamic range of approximately three decades (in shear rate) and can measure Newtonian, shear thinning, and yielding behaviors, which are representative of the different solution behaviors typically encountered. We compare our microliter capillary rheometer with existing instruments to describe the range of parameter space covered by our device. © 2014 Wiley Periodicals, Inc. and the American Pharmacists Association *J Pharm Sci* 104:678–685, 2015

Keywords: rheology; protein aggregation; viscosity; IgG antibody; microfluidics

INTRODUCTION

The protein therapeutic market is growing rapidly in sales and number of drugs available.¹ In early-stage formulation development, a wide variety of different solution conditions, including various excipients, buffers, and pH, are screened for various properties including viscosity. High protein concentrations are part of the manufacturing process; sometimes therapeutic protein solutions are concentrated up to approximately 250 g/L. High protein concentrations are also sometimes required for the drug product, as there is a limit to the volume of fluid that can be administered to the patient, for some methods such as subcutaneous injection.

Viscosity is a critical property not only because it relates directly to syringeability, but also because it is a relevant parameter for purification, fill/finish, and drug delivery.^{2,3} It is an indirect diagnostic of protein interactions and aggregation of the protein monomer.^{4–9} Although there is not a clearly established relationship between viscosity and protein self-association and/or aggregation, considerable work is aimed at this goal.¹⁰

Despite the maturity of viscometry, there remains a need for a rheometer that meets the following three needs of the biopharmaceutical industry: small volume; large dynamic range of shear rates; and no air–sample interface. The small volume requirement is particularly important to the biopharmaceutical industry during the screening stage of product develop-

ment. Traditional viscometric measurement methods include rotational rheometers such as the cone-and-plate, the cup-and-bob, or the double-gap cylinder geometries. The lower end of the volume range for these geometries is approximately 0.1, 3, and 4 mL, respectively, which places limits on the number of screening compounds that can be tested.

The requirement for a wide dynamic range in shear stems from the need for viscosity information in the high shear rate limit (e.g., shear rates greater than 10^5 s⁻¹) where syringeability is an issue and the concomitant need for low shear rate information (e.g., shear rates less than 100 s⁻¹), which relates to diffusive time scale of deformable structures.¹¹ The low shear rate range is particularly sensitive to the presence of irreversible aggregates.

Our third requirement of no air–fluid interface stems from work showing how the existence of such an interface in rotational rheometers sometimes complicates interpretation of results because of surface rheology and surface tension. The surface rheology complication¹² stems from the fact that the surface itself has an independent viscosity (units of Pa m s, as opposed to usual viscosity units of Pa s), which is convoluted with the viscosity measurement in situations that are common to protein therapeutics. The surface viscosity ranges significantly (from 10^{-9} to 10^{-5}) Pa m s for typical surfactants, and (from 10^{-5} to 10^{-2}) Pa m s for proteins (without added surfactant). If the surface rheology is measured separately with sufficient certainty, its effect can be accounted for.¹³ Unfortunately, these precision-limiting surface effects are typically more significant in the smaller-volume geometries. The other complication¹⁴ arises because surface tension serves as a major source of error in precision measurements at low torque because the nonaxisymmetric irregularities of the surface that frequently occur cause a net torque. Adding surfactant to the

Correspondence to: Steven D. Hudson (Telephone: +301-975-6579; Fax: +301-975-4924; E-mail: steven.hudson@nist.gov)

This article contains supplementary material available from the authors upon request or via the Internet at <http://wileylibrary.com>.

Journal of Pharmaceutical Sciences, Vol. 104, 678–685 (2015)

© 2014 Wiley Periodicals, Inc. and the American Pharmacists Association

solution reduces and often essentially eliminates the effects of both surface rheology and surface tension. Surfactants are added to therapeutic protein solutions also to stabilize them against aggregation.¹⁵

Pressure-driven capillary viscometry¹⁶ can meet the above three requirements; however, none to date have been designed and built to do so. The rheometer that we describe here measures the fluid viscosity over a wide range of shear rates (e.g., 1–10,000 s⁻¹) and temperatures (e.g., 0°C–80°C), yet it requires very small volumes (consuming ~3 μL at each temperature). In this report, we describe the approach and the resulting performance of this rheometer and then demonstrate its use to test protein solutions. We focus on the rheometer's capabilities and not on the rheological behavior of protein solutions, which can be explored with this instrument.

BACKGROUND

Here, we review the variety of viscometric techniques that are currently used to probe fluids under a wide range of conditions and discuss the relative merits with respect to the needs of the biopharmaceutical industry. Falling ball viscometry is sometimes used for protein solutions. The disadvantage is that the sample volume requirement is approximately 0.4 mL, and the shear rate range is typically limited. As the flow around the sphere is nonviscometric, the interpretation of this measurement is difficult when the fluid is non-Newtonian. In certain circumstances, when the diameter of the sphere is small compared with the cylinder containing the non-Newtonian fluid, and wall and end effects are eliminated, the zero-shear viscosity may be obtained by testing various spheres and extrapolating to zero stress, that is, to a sphere of infinitesimal size and neutral buoyancy.¹⁷ This procedure will not work for all fluids, for example, not for yield-stress fluids. Moreover, commercial instruments are typically designed with Newtonian fluids in mind, when it is not necessary to use multiple or small spheres.

One class of small-volume viscometers is oscillators. A variety of geometries and approaches have been tried.¹⁸ For many such cases, the so-called surface-loading limit¹⁹ applies, because the evanescent shear wave penetrates a small distance compared with the fluid gap (i.e., unlike in a typical rheometer that operates in the gap-loading limit, in which the shear propagates entirely across the gap). For kilohertz (kHz) oscillators,^{18,20} this penetration is roughly 10 μm or more, depending on viscosity. For megahertz (MHz) oscillators,^{21,22} however, the penetration is typically a few hundred nanometer, so that bulk viscosity is measured only for simple fluids and monomeric protein solutions, and they are not suitable for complex clustering protein solutions. MHz oscillators have been applied to such systems and qualitative effects of clustering have been observed, but the measurement is ill defined and inaccurate when the shear penetration layer is not large enough to sample the structures within the fluid. Recently, a microelectrical-mechanical (MEMs) microrheometer was reported, which is capable of low frequency behavior. As currently implemented, it contains an air–fluid interface that could act as a source of stress in protein solutions.²³

Optical methods based on diffusive motions of proteins or tracer particles have been recently introduced. For example, dynamic light scattering^{24,25} and particle tracking,^{26,27} which both take advantage of the generalized Stokes–Einstein re-

lation, GSER, need only very small volumes. The GSER is valid in some circumstances and not in others.²⁸ It fails whenever a probe particle changes the structure of the fluid to be measured.²⁹ This failure occurs in highly charged concentrated colloidal solutions,³⁰ of which protein solutions are a good example.³¹ Another failure occurs when the probe particle is small compared with the size of structures in the fluid. This happens whenever protein solutions form large aggregates and thus become heterogeneous.³¹ Guidelines involving a series of double checks to avoid the pitfalls of this method are elaborated by Amin et al.³²

Lastly, we discuss capillary rheometers where many are commercially available and smaller-volume versions have appeared recently.^{33,34} In a capillary rheometer, the flow is nonuniform (Poiseuille flow) but it is still viscometric. Even when the fluid is non-Newtonian, the shear stress and rate at the capillary wall is well defined provided the required Rabinowitsch correction (see Eq. (3) below) is made.³⁵ The basic principle underlying capillary viscometry is the Hagen–Poiseuille law describing nonturbulent flow through a tube:

$$R = \frac{\Delta P}{Q} = \frac{128 \eta L}{\pi d^4} = K\eta \quad (1)$$

As such, the pressure drop (ΔP) and flow rate (Q) must be measured to determine the hydrodynamic resistance (R) and the fluid viscosity (η). K is a constant that depends only on the length (L) and diameter (d) of a capillary. R and K can be calculated similarly when the capillary or channel has rectangular cross-section.³⁶ The performance of any given system, in terms of volume required and the range of accessible viscosities and shear rates, depends on K , on the dimensions of the capillary (and any input tubing), and on the sensitivity and range of measurement of ΔP and Q (see Table 1). Several microfluidic rheometers have been developed.^{33,37–45}

A recent capillary rheometer uses recirculation and thus enables dilution with the solvent or another solution mixture, in order to sample a whole range of concentration.⁴⁶ That

Table 1. Summary of Capability of Various Capillary and Microfluidic Rheometers Listed in Order of Approximate Sample Volume Consumed

Volume (μL)/Rate Sweep	η (mPa s)	$\dot{\gamma}_w$ (s ⁻¹) ^a	Reference
0.03	1 to 100	200 to 2000	39 ^b
1	0.2 to 100	200 to 2000	37
1	1 to 600	10 to 600	38 ^b
3	0.4 to 2000	10 to 3000	This work
10	0.9 to 100	10 to 1000	34
20	100 to 10 ⁹	1 to 1000	42 ^b
50	0.2 to 10 ⁵	1000 to 10 ⁵	33
100	0.2 to 10	100 to 2000	43
100	0.2 to 10	20 to 1000	45
750	0.2 to 1000	10 to 1500	46
1000	0.2 to 10	20 to 600	44
100,000	10 to 1000	1000 to 10 ⁶	40

^aThe shear rate range accessible to a single sample with a Newtonian viscosity in the middle of the rheometer's range. Note that a wider range of shear rate is usually accessible if the sample is non-Newtonian.

^bThese rheometers are based on tracking the interface between immiscible fluids. The pressure at the sample interface must be accounted for, whenever the applied pressure is low (i.e., comparable to the sample interface pressure).

Values of the current work are in bold.

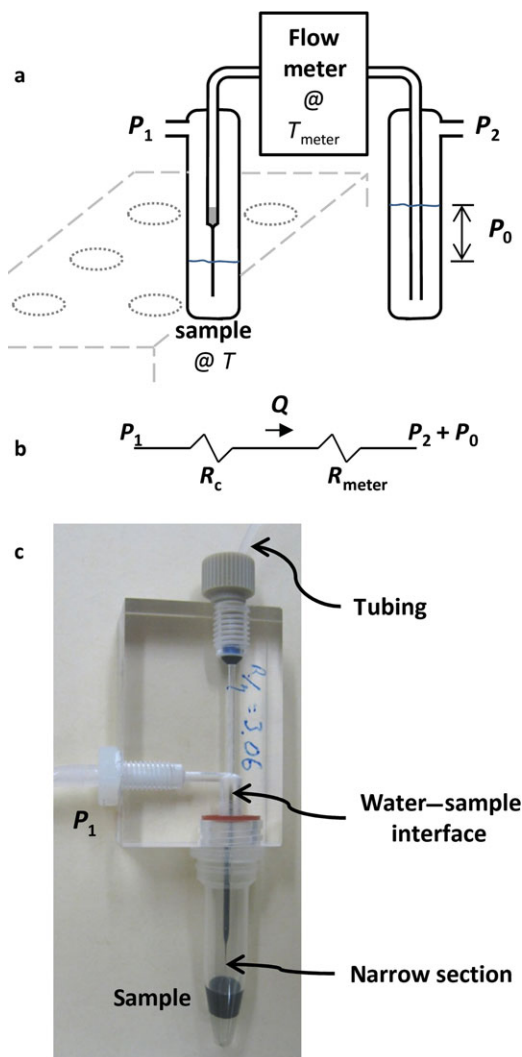


Figure 1. The instrument design. (a) Schematic of the apparatus, comprising two pressure chambers connected by polyethylene tubing through a flow meter. See text for details. The dotted and dashed lines near the sample chamber illustrate a possible modification whereby the sample pressure chamber may be fitted to dip into and seal onto a multiwell sample-and-reference plate. (b) Circuit schematic, illustrating two flow resistors (R_c and R_{meter} , the resistances of the capillary and meter, respectively) as described in the text. (c) Photograph of the sample fixture. The sample, here a black suspension of carbon nanotubes, is in a 0.5-mL Eppendorf tube that is threaded into a machined block of acrylic that holds a glass capillary, which is drawn to a narrow test portion at the bottom.

instrument's design requires weak mixing at the pressure taps, and there may be concerns over possible flow-induced changes in protein structure that affect results from one concentration to another. Table 1 contains a summary of capillary and microfluidic rheometers.

METHOD

Microcapillary Viscometry

Our implementation of a microcapillary rheometer is depicted in Figure 1. It comprises two pressure chambers, one containing sample and the other water, and a flow path in between.

The flow path includes a glass capillary with a narrow microcapillary tip, larger diameter polyethylene tubing, and the flow meter in series. Initially, the entire flow path is filled with water. Pressure is then used to drive sample through the microcapillary into the wider capillary, and if desired into the preflow meter polyethylene tubing, establishing a water–sample interface there. Measuring ΔP and Q , we obtain R and therefore η . The total pressure drop is $\Delta P = P_2 - P_1 + P_0$, where P_1 and P_2 are the pneumatic pressure of the sample and water reservoirs, respectively, and P_0 is the hydrostatic pressure because of their different elevations. Pressure can therefore be applied by either hydrostatic elevation or pneumatics, as described further below. The flow meter measures the volumetric flow rate (Q), which is the same through each of the components. The pressure drop during flow is not uniform, however, and is located primarily across the component of the flow path having the largest flow resistance, that is, the narrow microcapillary. This narrow tip is a length (L), typically 1–6 mm, of rather uniform diameter (d), typically 20–80 μm . L and d , and therefore K , are adjustable (see Supplementary Information, SI).

According to Eq. (1), a plot of pressure drop ($\Delta P = P_2 - P_1 + P_0$) versus Q has zero intercept. This constraint fixes the appropriate reference point for P_0 . As some sample fluids may be non-Newtonian and $\Delta P(Q)$ thus curved, interpolation to $Q = 0$ is carried out using small ΔP and Q at points roughly symmetrical about $Q = 0$. Reliable shift to zero intercept is thus obtained.

As all components of the flow path are in series, the total resistance is simply the sum of the components. The constant K_i of each element i is determined by calibration with fluids of known η . For convenience, we consider just two components in series: one filled with water and the other filled with sample. The portion filled with sample has a constant K_c associated essentially with the geometry of the narrow microcapillary, and the portion filled with water is all of the other components of the flow path summed together, having a constant K_{meter} . Equation (1) thus becomes:

$$R = \frac{\Delta P}{Q} = K_c \eta_s(T) + K_{\text{meter}} \eta_w(T_{\text{meter}}) \quad (2)$$

where the subscripts c and s refer to the microcapillary and sample, respectively. The subscript w denotes water. The sample is held in a temperature-controlled chamber (see SI). The sample temperature T reaches the set point within a $^\circ\text{C}$ after approximately 200 s and eventually is controlled within a few hundredths of a degree. Both temperatures T and T_{meter} are measured with Pt-resistance thermometers (RTDs).

The shear rate at the wall for Newtonian fluids is $\dot{\gamma}_a = \frac{32Q}{\pi d^3}$, and the shear stress at the wall is $\tau_{\text{wall}} = \eta_s \dot{\gamma}_a = \eta_s \frac{32Q}{\pi d^3} = \frac{\Delta P d}{4L}$. For non-Newtonian fluids, the shear rate at the wall is³⁵:

$$\dot{\gamma}_{\text{wall}} = \dot{\gamma}_a \left[\left(3 + \frac{d \ln \dot{\gamma}_a}{d \ln \tau_{\text{wall}}} \right) / 4 \right] \quad (3)$$

The expression inside the brackets is unity when the fluid is Newtonian. In subsequent references here to shear rate, the subscript wall is omitted for convenience.

Pressure (P_0 , P_1 , and P_2 ; see Fig. 1) is controlled by two methods in order to maximize the range. At the relatively high pressures (10^3 – 10^5 Pa), a computer-controlled multichannel

Fluigent MFCS (Villejuif, France) pneumatic controller is used. (Certain commercial materials and equipment are identified in this paper to adequately specify the experimental procedure. In no case does such identification imply recommendation or endorsement by the National Institute of Standards and Technology, nor does it imply that these are necessarily the best available for the purpose.) Over this range of pressures, the uncertainty remains essentially unchanged at ≈ 30 Pa. For lower pressures (3–7000 Pa), P_1 and P_2 are set to ambient (open to air) and a computer-controlled motorized stage (Zaber, Vancouver, BC, Canada, A-LST1500D) is used to elevate the water reservoir (to change P_0). This stage has a step size of ≈ 2 μm and a large travel-relative displacement accuracy of approximately ± 0.00013 . Displacements are repeatable, returning to the same step position. These characteristics mean that the uncertainty for small displacements is ≈ 0.02 Pa and up to 2 Pa for large displacements.

Flow was measured using a Fluigent Flowcell meter based on flow-induced thermal convection. This device comprises a tube ($d \approx 150$ μm , $L \approx 3$ cm) fitted with a small heater flanked upstream and downstream by two thermocouples. Flow through the channel convects heat downstream, causing a temperature differential whose magnitude correlates to flow rate. The meter can measure flow rates from approximately ± 0.1 to ± 120 nL/s. Capabilities of the meter are elaborated in SI.

Operation of the microcapillary rheometer and data acquisition are handled by a program written in LabVIEWTM. Continuous acquisition of flow rate and pressure data is communicated to the rest of the program in packets, so that data acquisition is not interrupted by other functions such as analysis, operation, or writing to disk. This approach ensures an accurate record of the total amount of sample that passes into the instrument. The residual sample volume that must remain in the sample reservoir can be very small (~ 10 μL has been achieved) when the microcapillary is positioned at the bottom of the reservoir.

In general, the sample may be either miscible or immiscible with water. When the sample is immiscible with water, a small additional pressure is required to move the sample-to-water interface.³⁹ Most of our experience is with samples that are miscible with water. In this latter case, that is, the exclusive interest of this report, the interfacial effect vanishes, but sample dispersion and miscible displacement must be considered. Dispersion is most significant whenever a low-viscosity fluid pushes into a higher viscosity one, because it occurs by the viscous fingering mechanism.^{48,49} For example, when the sample is more viscous than water, the flow front is stable while the sample is drawn in, but viscous fingering occurs when the flow is reversed. At large Peclet number, that is, when flow is much faster than diffusion, the practical limit of expulsion is $\approx 40\%$ – 50% of the volume drawn in, depending on the viscosity ratio.⁴⁹ After that, the sample in the narrow section would be diluted by water. The pumping protocol is designed to avoid any condition when sample dispersion dilutes the sample in the narrow section of the capillary.

Other Viscometry Measurements

Other capillary viscosity measurements were used for validation. Here, we use a commercial rheometer (m-VROCTM; RheoSense, San Ramon, CA) that has a series of pressure sensors embedded along the microchannel to measure a pressure gradient ($\Delta P/L$). The flow rate is controlled with a sy-

ringe pump. Different pressure sensors are available for different ranges; here types A and D sensors were used. For samples with a viscosity of approximately 3 mPa s, this instrument is useful for flow rates in the range approximately 1000–100,000 s^{-1} .³³

Fluids

Fluids used for this study were distilled water, anhydrous glycerol (Mallinckrodt Baker, St. Louis, MO, used as received) and a monoclonal antibody (mAb). Various concentrations (up to 120 g/L) of the mAb were prepared using ultrafiltration/diafiltration at two pH, one in a bicine buffer at pH 8.7 near the isoelectric point and the other at pH 6 in histidine buffer. The concentration was measured by absorption at 280 nm (A280) using an Agilent (Santa Clara, CA) 8453 UV-Visible spectrophotometer with an absorption coefficient of $\epsilon_{280} = 1.47$ L/(g cm). Other characteristics of the protein solutions are not reported here, consistent with the focus of this report being on the new rheometer. Protein solutions were stored for several months between 2°C and 8°C, and allowed for 1 h to come to room temperature before removing a sample for testing.

RESULTS AND DISCUSSION

To characterize the rheology of a protein in solution at a certain pH and salt or excipient concentration, we desire to explore three main variables: shear rate, protein concentration, and temperature. Here, we illustrate that this new rheometer can effectively study these three variables (in Figs. 2–4), and we leave to future work the task of correlating biophysical and rheological properties.

Additional background concerning the rheometer is published in SI. Specifically, the statistical behavior of the flow meter and the data acquisition strategies are described; these strategies permit the rheometer to measure a wide range of shear rate and to consume such small volumes of fluid. Calibration of the geometrical factors K_{meter} and K_c is also reported in SI. Consistency of calibration at different temperature demonstrates that the sample temperature is well controlled.

To test this calibration, the viscosity of glycerol was measured, with results consistent with those published in the literature (Table 2).⁵¹ This agreement confirms not only the accuracy of the rheometer but also validates the instrument's design. Specifically, it shows that a more viscous sample is able to satisfactorily displace the water as it is drawn slowly (300 nL at ~ 2 nL/s) from the sample reservoir into the microcapillary. Glycerol is a particularly sensitive test, as a noticeable 5% reduction in viscosity is anticipated if the glycerol at the capillary surface is mixed with and diluted by merely 0.3% mass fraction of water.⁵¹ Instead, the rheometer reports random positive

Table 2. Glycerol Viscosity

T (°C)	η (mPa s) Literature ⁵⁰	η (mPa s) Measured	Difference (%)
20	1410	1470 \pm 20	+4.4
30	612	610 \pm 10	-0.3
40	284	281 \pm 9	-1.1
50	142	144 \pm 3	+1.5
60	81.3	81.9 \pm 2.2	+0.8
70	50.6	49.1 \pm 1.2	-2.9

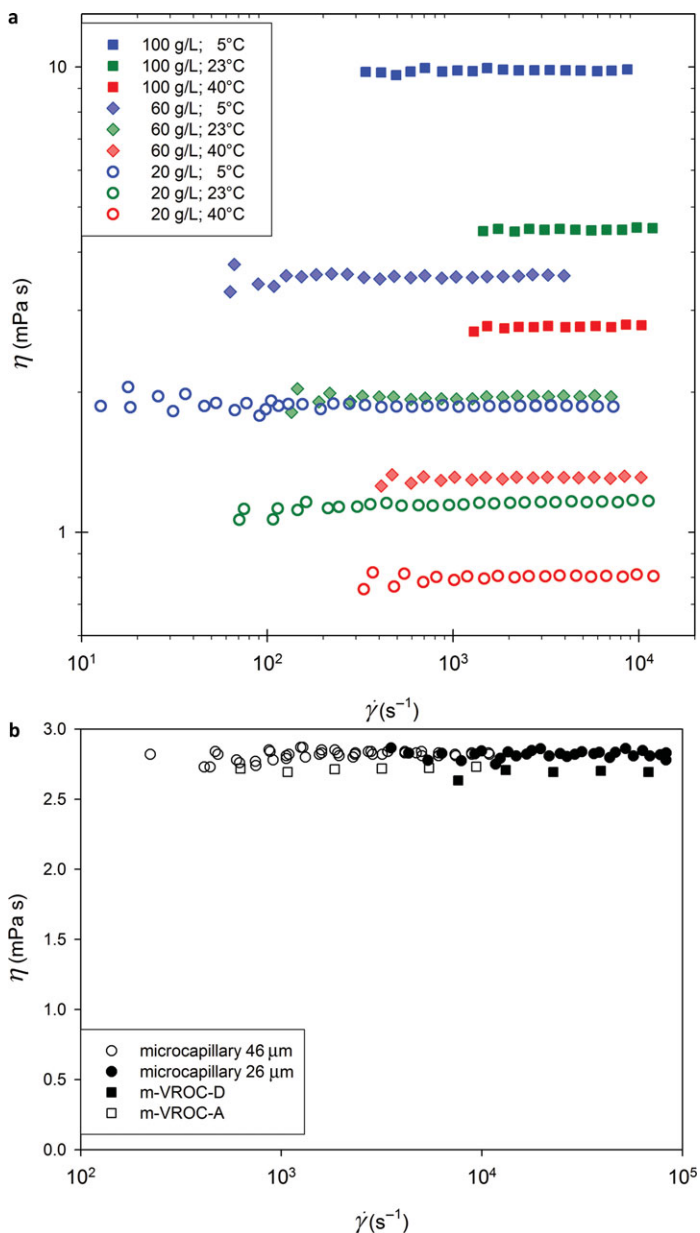


Figure 2. Viscosity $\eta(\dot{\gamma})$ of antibody solutions, over a range of shear rates. (a) Antibody solutions at pH 8.7 and temperatures 5°C, 23°C and 40°C, illustrating Newtonian behavior. (b) Antibody solution at pH 6.0 and 23°C comparing results from the microcapillary (circles) and m-VROC (square) rheometers. Open and closed symbols represent two different capillaries (open: $d = 46 \mu\text{m}$; closed: $d = 26 \mu\text{m}$) and two different m-VROC chips (open: chip A; closed: chip D), see text. Shear rate is determined according to Eq. (3).

and negative deviations that are generally a few percent or less (Table 2). Miscible displacement of fluids (where the more viscous one invades the other) is therefore a suitable approach for microcapillary rheometry.

On the basis of the calibration, the effective diameter d of a glass capillary microchannel can be approximated from an estimate of its length L . As the resistance is proportional to Ld^{-4} see Eq. (1), this approximation of d is quite accurate. From knowledge of d , the true shear rate at the microcapillary wall may be determined see Eq. (3).

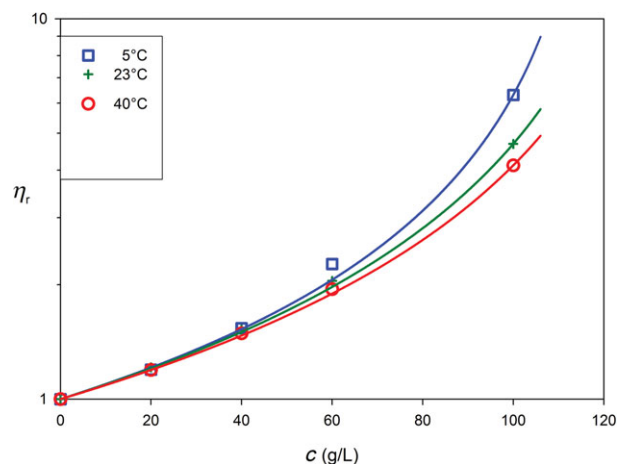


Figure 3. Concentration dependence of the relative viscosity η_r of mAb solutions at pH 8.7 for three different temperatures, 5°C, 23°C, and 40°C. The lines are fits to the Krieger Dougherty model.

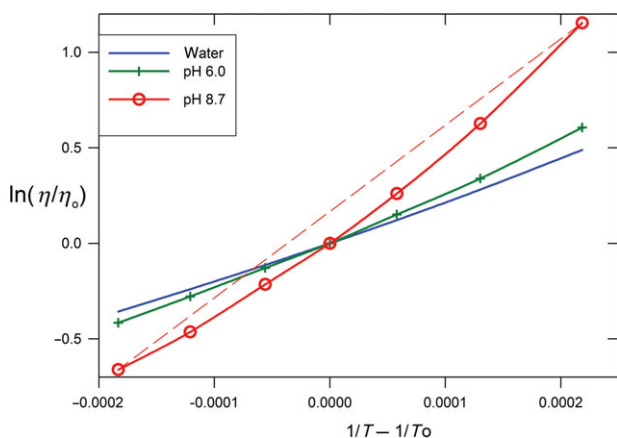


Figure 4. Viscosity $\ln(\eta/\eta_0)$ v. $1/T - 1/T_0$ of 120 g/L mAb solutions at pH 6.0 and 8.7 and $T_0 = 23^\circ\text{C}$. Water literature data are shown for reference.⁵⁰ The straight dashed line connecting endpoints of the pH 8.7 data is to emphasize its curvature.

Having calibrated the viscosity and the true shear rate, we now report the viscosity of protein solutions to illustrate the performance of the rheometer. First, we explore the effect of shear rate (Fig. 2). Nearly a three decade span in shear rate can be obtained see Fig. 2a; 20 g/L at 5°C). The total volume consumed for the measurements reported in Fig. 2a was 11.3, 5.7, and 7.5 μL for the solutions of concentration 20, 60, and 100 g/L, respectively. Over this wide range of shear rate, all of the antibody solutions here exhibit Newtonian behavior: specifically, the bracketed quantity in Eq. (3) is found to be 1.000 ± 0.002 . Of course, the need to measure a wide range of shear rate is because not all antibody solutions are Newtonian, as illustrated in a recent report by Zarraga et al.⁵² Indeed, we have tested heavily aggregated antibody solutions that exhibit shear yielding (not reported here). Other complex fluids too have been tested with this microcapillary rheometer, and a wide variety of non-Newtonian behavior has been recorded (not reported here). By exploring a range of shear rate, the rheometer is sensitive to the effects of structure within complex fluids.

Next, we compare data from another rheometer (Fig. 2b). The average viscosity reported by the microcapillary

rheometer is 2.82 ± 0.04 mPa s. This is approximately 4% higher than the viscosity of the same solution measured by the m-VROC rheometer, 2.70 ± 0.03 mPa s. The uncertainty reported in each instance is one standard deviation. RheoSense reports that the accuracy of the m-VROC is $\pm 2\%$. Each rheometer was calibrated with water using the data of Kestin et al.⁵⁰ for reference. This calibration causes each rheometer to give self-consistent results, with different test channels, even though, for example, the micro capillary diameter differs markedly (see Fig. 2 caption). In summary, the two rheometers are in near agreement. Future work may determine whether the observed 4% difference in this instance is systematic or random.

The next main variable to explore is protein concentration. For this, we report the relative viscosity η_r (of the sample relative to that of the buffer) of the antibody solutions at a pH of 8.7, that is, near its isoelectric point (Fig. 3). The viscosity rises dramatically with increasing concentration, especially as it approaches some critical value at higher concentration. Such is roughly the behavior of all particle dispersions. Although model hard sphere colloidal solutions follow ideal nonassociating models such as the Krieger Dougherty equation,⁵³ these models do not apply readily to protein solutions,⁵⁴ which have various degrees of self association. Modest deviations from the Krieger Dougherty model are already apparent in Fig. 3, and more significant deviations have been observed.

The final variable to explore is temperature, whose effect was already illustrated in Figures 2 and 3. Now we explore the effect of temperature in more detail. For simple fluids, the effect of temperature is often well described by the Arrhenius equation. In this view, flow is an activated process and the friction between molecules depends exponentially on temperature: $\ln(\eta)$ is proportional to $E_a/(RT)$, where E_a is the activation energy, and R is the gas constant. A plot of $\ln(\eta/\eta_0)$ v. $1/T - 1/T_0$ (where the subscript 0 signifies any reference point, here 23°C) is therefore informative to evaluate whether fluids exhibit such behavior. The viscosity of fluids departs from this simple description whenever molecules associate with one another. Such is the case for water approaching its freezing point. Stronger effects are observed in supercooled liquids. Protein solutions may also exhibit nearly Arrhenius behavior; the apparent activation energy depends on the protein, its concentration, and other solution compositions.⁵⁵

Here, we compare two concentrated antibody solutions at pH 6.0 and pH 8.7 (Fig. 4), the latter being near to the pI, measured at seven different temperatures between 5°C and 40°C. These data were obtained consuming only 9.3 μ L of one solution and 21.8 μ L of the other. These data are well fit by a second-order expansion in terms of $1/(RT) - 1/(RT_0)$. The linear coefficient is the activation energy E_a and the second-order term measures the departure from Arrhenius' equation. For pure water at 23°C,⁵⁰ the activation energy (E_a) and the second-order coefficient are 17.26 ± 0.03 kJ/mol and 51.0 ± 1.7 (kJ/mol)², respectively. For comparison, these coefficients for the antibody solutions can be expressed relative to those of water. The normalized activation energies are thus 1.20 ± 0.01 and 2.09 ± 0.01 , for pH 6.0 and 8.7, respectively. The corresponding normalized second-order coefficients are 1.7 ± 0.2 and 5.6 ± 0.3 . The apparent friction between antibodies and the degree to which they associate with one another are therefore much stronger at pH 8.7. Although data such as this may be useful in future understanding of the

effects of monomer association in concentrated protein solutions, we leave to future publications to discuss and explore the implications.

Here, we simply demonstrate the utility of this rheometer. Specifically, it is suitable to obtain such data from small quantities (of order 10 μ L) of solution. It can explore the rheology of protein solutions of various composition as a function of major variables of shear rate, concentration, and temperature.

CONCLUSIONS AND OUTLOOK

Although capillary rheometry is well established, here we demonstrate a unique implementation that meets needs of the biopharmaceutical industry: small volume; large dynamic range of shear rates; and no air-sample interface. Here, we demonstrate that accurate viscosities, ranging from 0.5 to 2000 mPa s with uncertainty of a few percent, can be measured over a (two or more decade) wide range of shear rate with just a few microliters of solution. Various experimental protocols (see SI) are necessary to achieve this accuracy and performance.

Viscosities of antibody solutions were measured as a function of shear rate, protein concentration, and temperature. These measurements demonstrate the utility of the rheometer for characterizing some of the solution behavior of proteins.

In the approach that we outline here, sample loading is trivial: the microcapillary is simply dipped into the sample vial. On the basis of this simplicity, interfacing with a multiwell plate would be straightforward, as noted in Figure 1. Such adaptation seems desirable in light of industrial requirements that call for testing of multiple different formulations and solution conditions.

ACKNOWLEDGMENTS

The following contributions are gratefully recognized: excellent machining by Chris Amigo (NIST) and protein purification by Justin Weaver (MedImmune). This work was performed under a Cooperative Research and Development Agreement (CRADA) between NIST and MedImmune. Under the terms of the CRADA, this document may not be used as advertising for any product or service, nor may MedImmune imply to anyone that the CRADA of the research results are an endorsement by NIST of any MedImmune products or services.

REFERENCES

- Chan AC, Carter PJ. 2010. Therapeutic antibodies for autoimmunity and inflammation. *Nat Rev Immunol* 10(5):301–316.
- Shire SJ, Shahrokh Z, Liu J. 2004. Challenges in the development of high protein concentration formulations. *J Pharm Sci* 93(6):1390–1402.
- Rathore N, Pranay P, Bernacki J, Eu B, Ji WC, Walls E. 2012. Characterization of protein rheology and delivery forces for combination products. *J Pharm Sci* 101(12):4472–4480.
- Jachimska B, Wasilewska M, Adamczyk Z. 2008. Characterization of globular protein solutions by dynamic light scattering, electrophoretic mobility, and viscosity measurements. *Langmuir* 24(13):6866–6872.
- Johnston KP, Maynard JA, Truskett TM, Borwankar AU, Miller MA, Wilson BK, Dinin AK, Khan TA, Kaczorowski KJ. 2012. Concentrated dispersions of equilibrium protein nanoclusters that reversibly dissociate into active monomers. *ACS Nano* 6(2):1357–1369.

6. Kiefhaber T, Rudolph R, Kohler HH, Buchner J. 1991. Protein aggregation in vitro and in vivo—A quantitative model of the kinetic competition between folding and aggregation. *Nat Biotechnol* 9(9):825–829.
7. Tessier PM, Wu JM, Dickinson CD. 2014. Emerging methods for identifying monoclonal antibodies with low propensity to self-associate during the early discovery process. *Expert Opin Drug Deliv* 11(4):461–465.
8. Liu J, Nguyen MDH, Andya JD, Shire SJ. 2005. Reversible self-association increases the viscosity of a concentrated monoclonal antibody in aqueous solution. *J Pharm Sci* 94(9):1928–1940.
9. Connolly BD, Petry C, Yadav S, Demeule B, Ciaccio N, Moore JMR, Shire SJ, Gokarn YR. 2012. Weak interactions govern the viscosity of concentrated antibody solutions: High-throughput analysis using the diffusion interaction parameter. *Biophys J* 103(1):69–78.
10. Cheng WQ, Joshi SB, Jain NK, He F, Kerwin BA, Volkin DB, Mid- daugh CR. 2013. Linking the solution viscosity of an IgG2 monoclonal antibody to its structure as a function of pH and temperature. *J Pharm Sci* 102(12):4291–4304.
11. Larson RG. 1999. *The structure and rheology of complex fluids*. New York: Oxford University Press.
12. Sharma V, Jaishankar A, Wang Y-C, McKinley GH. 2011. Rheology of globular proteins: Apparent yield stress, high shear rate viscosity and interfacial viscoelasticity of bovine serum albumin solutions. *Soft Matter* 7(11):5150–5160.
13. Castellanos MM, Pathak JA, Colby RH. 2014. Both protein adsorption and aggregation contribute to shear yielding and viscosity increase in protein solutions. *Soft Matter* 10(1):122–131.
14. Johnston MT, Ewoldt RH. 2013. Precision rheometry: Surface tension effects on low-torque measurements in rotational rheometers. *J Rheology* 57(6):1515–1532.
15. Garidel P, Hoffmann C, Blume A. 2009. A thermodynamic analysis of the binding interaction between polysorbate 20 and 80 with human serum albumins and immunoglobulins: A contribution to understand colloidal protein stabilisation. *Biophys Chem* 143(1–2):70–78.
16. Kestin J, Sokolov M, Wakeham W. 1973. Theory of capillary viscometers. *Appl Sci Res* 27(1):241–264.
17. Gottlieb M. 1979. Zero-shear-rate viscosity measurements for polymer-solutions by falling ball viscometry. *J Non-Newton Fluid Mech* 6(2):97–109.
18. Willenbacher N, Oelschlaeger C. 2007. Dynamics and structure of complex fluids from high frequency mechanical and optical rheometry. *Curr Opin Colloid Interface Sci* 12(1):43–49.
19. Schrag JL. 1977. Deviation of velocity-gradient profiles from gap loading and surface loading limits in dynamic simple shear experiments. *Trans Soc Rheol* 21(3):399–413.
20. Fritz G, Pechhold W, Willenbacher N, Wagner NJ. 2003. Characterizing complex fluids with high frequency rheology using torsional resonators at multiple frequencies. *J Rheol* 47(2):303–319.
21. Saluja A, Badkar AV, Zeng DL, Nema S, Kalonia DS. 2006. Application of high-frequency rheology measurements for analyzing protein-protein interactions in high protein concentration solutions using a model monoclonal antibody (IgG(2)). *J Pharm Sci* 95(9):1967–1983.
22. Saluja A, Kalonia DS. 2004. Measurement of fluid viscosity at microliter volumes using quartz impedance analysis. *AAPS Pharm- SciTech* 5(3):68–81.
23. Christopher GF, Yoo JM, Dagalakis N, Hudson SD, Migler KB. 2010. Development of a MEMS based dynamic rheometer. *Lab Chip* 10(20):2749–2757.
24. Segre PN, Meeker SP, Pusey PN, Poon WCK. 1995. Viscosity and structural relaxation in suspensions of hard-sphere colloids. *Phys Rev Lett* 75(5):958–961.
25. He F, Becker GW, Litowski JR, Narhi LO, Brems DN, Razinkov VI. 2010. High-throughput dynamic light scattering method for measuring viscosity of concentrated protein solutions. *Anal Biochem* 399(1):141–143.
26. Mason TG, Weitz DA. 1995. Optical measurements of frequency-dependent linear viscoelastic moduli of complex fluids. *Phys Rev Lett* 74(7):1250–1253.
27. Tu RS, Breedveld V. 2005. Microrheological detection of protein unfolding. *Phys Rev E* 72(4):041914.
28. Squires TM, Mason TG. 2010. *Fluid mechanics of microrheology*. *Annu Rev Fluid Mech* 42:413–438.
29. Solomon MJ, Lu Q. 2001. Rheology and dynamics of particles in viscoelastic media. *Curr Opin Colloid Interface Sci* 6(5–6):430–437.
30. Horn FM, Richtering W, Bergenholtz J, Willenbacher N, Wagner NJ. 2000. Hydrodynamic and colloidal interactions in concentrated charge-stabilized polymer dispersions. *J Colloid Interface Sci* 225(1):166–178.
31. Wagner M, Reiche K, Blume A, Garidel P. 2013. Viscosity measurements of antibody solutions by photon correlation spectroscopy: An indirect approach—Limitations and applicability for high-concentration liquid protein solutions. *Pharm Dev Technol* 18(4):963–970.
32. Amin S, Rega CA, Jankevics H. 2012. Detection of viscoelasticity in aggregating dilute protein solutions through dynamic light scattering-based optical microrheology. *Rheol Acta* 51(4):329–342.
33. Pipe CJ, Majmudar TS, McKinley GH. 2008. High shear rate viscometry. *Rheol Acta* 47(5–6):621–642.
34. Goodall D. 2013. Viscosity measurement apparatus and method. US Patent 20130186184.
35. Weissenberg K, as cited by Rabinowitsch B. 1929. On the viscosity of elasticity of brines. *Zeitschrift Fur Physikalische Chemie-Abteilung a-Chemische Thermodynamik Kinetik Elektrochemie Eigenschaftslehre* 145(1):1–26.
36. Berker R. 1963. Integration des equations du mouvement d'un fluide visqueux incompressible. In *Handbuch der Physik; Flugge S, Truesdell CA, Eds. Vol 8. Part 2, Fluid dynamics*. Berlin, Germany: Springer-Verlag, pp 1–384.
37. Srivastava N, Davenport RD, Burns MA. 2005. Nanoliter viscometer for analyzing blood plasma and other liquid samples. *Anal Chem* 77(2):383–392.
38. Srivastava N, Burns MA. 2006. Analysis of non-Newtonian liquids using a microfluidic capillary viscometer. *Anal Chem* 78(5):1690–1696.
39. Livak-Dahl E, Lee J, Burns MA. 2013. Nanoliter droplet viscometer with additive-free operation. *Lab Chip* 13(2):297–301.
40. Kang K, Lee LJ, Koelling KW. 2005. High shear microfluidics and its application in rheological measurement. *Exp Fluid* 38(2):222–232.
41. Abkarian M, Faivre M, Stone HA. 2006. High-speed microfluidic differential manometer for cellular-scale hydrodynamics. *Proc Natl Acad Sci USA* 103(3):538–542.
42. Moon D, Bur AJ, Migler KB. 2008. Multi-sample micro-slit rheometry. *J Rheol* 52(5):1131–1142.
43. Choi S, Park JK. 2010. Microfluidic rheometer for characterization of protein unfolding and aggregation in microflows. *Small* 6(12):1306–1310.
44. Kang YJ, Yoon SY, Lee KH, Yang S. 2010. A highly accurate and consistent microfluidic viscometer for continuous blood viscosity measurement. *Artif Organs* 34(11):944–949.
45. Kang YJ, Yang S. 2013. Integrated microfluidic viscometer equipped with fluid temperature controller for measurement of viscosity in complex fluids. *Microfluid Nanofluid* 14(3–4):657–668.
46. Grupi A, Minton AP. 2012. Capillary viscometer for fully automated measurement of the concentration and shear dependence of the viscosity of macromolecular solutions. *Anal Chem* 84(24):10732–10736.
47. Morrison FA. 2001. *Understanding rheology*. New York, NY: Oxford University Press.
48. Petitjeans P, Maxworthy T. 1996. Miscible displacements in capillary tubes .1. Experiments. *J Fluid Mech* 326:37–56.
49. Chen CY, Meiburg E. 1996. Miscible displacements in capillary tubes .2. Numerical simulations. *J Fluid Mech* 326:57–90.

- 50.** Kestin J, Sokolov M, Wakeham WA. 1978. Viscosity of liquid water in range -8-degrees-c to 150-degrees-c. *J Phys Chem Ref Data* 7(3):941–948.
- 51.** Segur JB, Oberstar HE. 1951. Viscosity of glycerol and its aqueous solutions. *Ind Eng Chem* 43(9):2117–2120.
- 52.** Zarraga IE, Taing R, Zarzar J, Luoma J, Hsiung J, Patel A, Lim F. 2013. High shear rheology and anisotropy in concentrated solutions of monoclonal antibodies. *J Pharm Sci* 102(8):2538–2549.
- 53.** Krieger IM, Dougherty TJ, 1959. A mechanism for non-Newtonian flow in suspensions of rigid spheres. *Trans. Soc. Rheol.* 3:137–152.
- 54.** Sarangapani PS, Hudson SD, Migler KB, Pathak JA. 2013. The limitations of an exclusively colloidal view of protein solution hydrodynamics and rheology. *Biophys J* 105(10):2418–2426.
- 55.** Monkos K, Turczynski B. 1999. A comparative study on viscosity of human, bovine and pig IgG immunoglobulins in aqueous solutions. *Int J Biol Macromol* 26(2–3):155–159.

A Microliter Capillary Rheometer for Characterization of Protein Solutions

S. D. Hudson,^{1,a)} P. Sarangapani,² J. A. Pathak², K. B. Migler¹

¹*Polymers and Complex Fluids Group, Materials Science and Engineering Division, National Institute of Standards and Technology, 100 Bureau Dr., Gaithersburg, MD 20899*

²*Formulation Sciences, MedImmune, One MedImmune Way, Gaithersburg, MD 20878*

MICROCAPILLARY FORMATION

The micro capillaries were drawn from a type-1 class-A borosilicate glass capillary (Sutter Instrument) with an inside diameter of 780 μm , using a Sutter Instrument P-2000 micropipette puller. The diameter and length of the resulting narrow section of the capillary can be adjusted with drawing conditions and forging, i.e. fracturing or blowing of the tip, using an MFG-5AP microforge from Microdata Instruments. Glass blowing creates a gentler entrance at the tip. Due to the nature of the drawing process, the drawn section of the microcapillary is quite, but not exactly, uniform in cross section. Typical dimensions of this nearly uniform section are d ranging (20 to 80) μm and L ranging (1 to 6) mm, with L/d ranging 50 to 300.

During sample testing, flow through the micro capillary is accompanied by extensional flow at the entrance and exit. The effect of these entrance and exit flows is included in calibration of K , and they could be evaluated further by adjusting the ratio L/d systematically.

By choosing different capillaries to adjust K (see Eq 1), the range of shear rates and of viscosities accessible is adjustable.

HYDROSTATIC PRESSURE

Hydrostatic pressure is described here by P_0 . An additional hydrostatic pressure arises when the sample density differs from water. In the present report, this pressure is at most 0.1 % of the driving pressure drop ΔP , and thus is neglected.

SAMPLE CHAMBER

The temperature-controlled chamber for the sample comprised two thin inner aluminum boxes (not shown) surrounding the Eppendorf tube (Fig. 1 a), and the entire assembly was enclosed in an outer metal box, with rigid-foam insulation on 3 sides and two Peltier elements (cooled by a water circulator) on the

4th side. When the Peltier elements are powered, the characteristic time response of the temperature in the inner-most chamber is ≈ 250 s. More intimate contact between a temperature controlled housing and the sample would be necessary to speed temporal response. Here we used feed-forward control¹ of the Peltier power when T differs significantly from the set point and normal PD feedback control after T approaches the set point. The balance between feed-forward and feedback changes smoothly according to a Gaussian distribution about the set point. The sample temperature reaches within a $^\circ\text{C}$ after approximately 200 s and eventually is controlled within a few hundredths of a degree.

FLOW METER STATISTICS

The primary measurements of the rheometer are flow rate Q and pressure drop ΔP . Since the uncertainty of the pressure is relatively small, the greater source of uncertainty is the flow meter. To achieve the broadest possible shear rate range requires efficient data averaging and statistical analysis of the flow meter output (Fig. S1). These measurements and analysis determine the optimal setting for the flow meter resolution, i.e. the number n of significant bits in the numerical output, ranging from 9 to 15. The flow rate can be read at various bits of resolution, and the highest precision (of the mean flow rate) is achieved at the lowest resolution (9 bits).

This perhaps surprising result is because the coarsest resolution remains finer than the random measurement noise, and the rate of data acquisition is fastest at lowest meter resolution. The cost of increased resolution is increased measurement time, which ranged from 2 ms to 36 ms per measurement. For each resolution setting, multiple data points were accumulated and analyzed statistically. The total time of data accumulation is directly proportional to the volume of fluid that passes through the meter, which is a matter of prime concern since our objective is to reduce the amount of fluid required for viscosity

^{a)} steven.hudson@nist.gov

Official contribution of the National Institute of Standards and Technology; not subject to copyright in the United States.

measurement. For this comparison (Fig. S1), the total time of data accumulation was fixed at 18 s. The total number of data points N thus ranged from 9000 (at 9 bit) to 500 (at 15 bit). Data was accumulated under three conditions such that the flow meter was: empty (dry), filled with water (with zero pressure drop), and filled and pressurized so that water flowed through the meter at a rate of approximately 100 nL/s. Actually, a range of flow conditions were recorded, and we report the condition at 100 nL/s as representative. For each data set, we computed its standard deviation σ . At zero pressure drop, this σ_0 represents the noise floor (often expressed in terms of percent full scale), and at high flow rate σ_{100} reflects uncertainty of the gain (often expressed as % of signal).

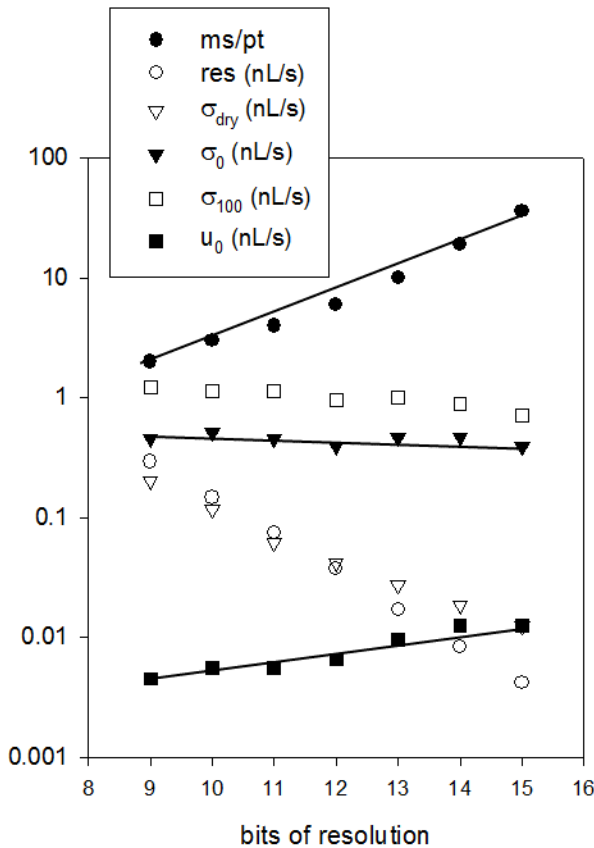


FIG. S1. Flow meter performance, with data acquired with various bits of resolution. Plotted here are the time in ms required to obtain each flow rate reading (ms/pt), the numerical resolution (res), the standard deviation of flow rate readings when the flow meter is dry (σ_{dry}), wet and no differential pressure (σ_0) and wet with average flow rate of ≈ 100 nL/s (σ_{100}), and u_0 ($= \sigma_0/\sqrt{N}$) the standard uncertainty of the mean of as many data points that can be obtained in 18 s. The lines are guides for the eye.

Our primary interest is u , the uncertainty of the mean, which is simply σ/\sqrt{N} . While more data bits means finer numerical resolution, best performance is with the lowest (9-bit) resolution, since σ is relatively insensitive to the bit resolution, and thus u is reduced primarily by accumulating larger N . Data acquisition rate is thus a premium. Specifically, various data associated with flow rate measurements (Fig S1) approximate exponential functions, with a power proportional to n . The numerical resolution of course is proportional to 2^{-n} . The exponents for the time per measurement and of σ are roughly $0.69n$ and $-0.03n$ (Fig S1) respectively, so that the uncertainty u increases with increasing resolution with an exponent of $\approx 0.27n$. This circumstance arises because the standard deviation of the flow meter readings when filled with water is always greater than numerical resolution. Best performance is obtained therefore with the lowest (9-bit) resolution, to maximize data acquisition rate.

The standard deviation σ is sensitive to disturbances (such as vibrations, blowing air, and temperature variations). For example, when the dc power supply for the sample temperature chamber was nearby, σ increased approximately three fold when the power supply was switched on. Therefore we used a vibration isolation table and kept fans distant. Better rheometer performance rests on reducing σ as much as possible.

IDENTIFYING STEADY-STATE FLOW CONDITIONS

Discarding transient data efficiently is crucial for small volume performance. This challenge arises because whenever switching the pressure drop $\Delta P = P_2 - P_1 + P_0$ to a new state, an oscillation in the flow rate follows. We therefore implemented a scheme to decide efficiently when steady state is reached.

We remind the reader that the flow rate is measured at a distance from the glass capillary microchannel, so that the transients may also represent extraneous effects for example arising from various sources of apparent compressibility.

To efficiently assess if the flow reading is steady, we use the following algorithm, which allows for integration times as long as desired, but minimal time sampling transients (Fig. S2). The data is collected in packets (e.g., $N_1 = 100$ data points at a time) into an accumulated set. Initially, the set is empty. After two sets are accumulated, we calculate the mean value of the oldest packet \bar{Q}_o and compare it to the mean of the entire accumulated set \bar{Q} . The oldest packet is retained only if its mean satisfies this inequality:

$$\bar{Q} - cu_q^e < \bar{Q}_o < \bar{Q} + cu_q^e \quad , \quad (S1)$$

where u_q^e is the expected uncertainty of the measurement (based on the meter resolution and the flow rate, see Fig S1), and c is an adjustable constant, which regulates the stringency of this criterion. This approach ensures that the oldest packet is representative of the entire accumulated set. When c is chosen to be 2 (as usually done here), it means that the oldest packet is retained if it represents 95 % of the accumulated packets. If the inequality fails, then the oldest packet is removed from the accumulated set. Either way, the algorithm proceeds until the accumulated set contains the desired number of data packets (e.g., 100 steady data packets) to reduce u far below σ . In this way, measurements of flow rate with 1 % accuracy can be obtained even when the flow rate is as small as the noise σ . This approach is necessary to acquire even a modest range of shear rates.

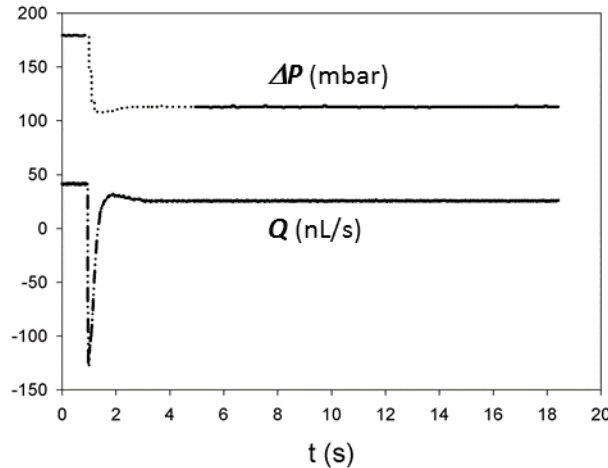


FIG. S2. $\Delta P(t)$ and $Q(t)$, showing transient (dotted) and steady (solid line) readings.

CALIBRATION DATA

The geometrical factors K_{meter} and K_c can be calibrated with water, or other standards. First, K_{meter} is obtained by operating the rheometer with a glass capillary that was not formed into a microchannel. In this case, the flow resistance of the capillary is negligible compared to the rest of the system, whose primary resistance is the flow meter. Dividing the flow resistance by the viscosity of water² in the flow meter, the data K_{meter} is plotted in Figure S3, and statistical analysis gives $K_{meter} = (2763 \pm 36) \text{ nL}^{-1}$ (where the uncertainty is \pm one standard deviation).

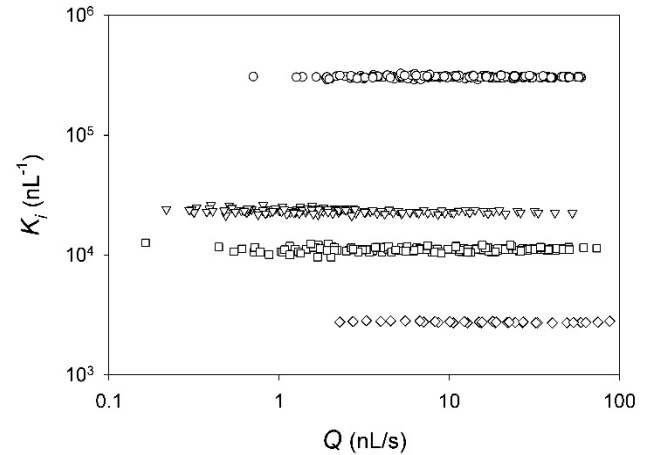


FIG. S3. Calibration data of K_{meter} (the lowest data set) and K_c for three microcapillaries (upper sets), each of which has essentially a fixed value, independent of temperature or viscosity. Within these sets are data obtained at the following temperatures: (5, 12, 20, 29, 40, 52, 65, and 70) °C

Having determined K_{meter} , Eqn 3 can then be applied to calibrate K_c of each forged microcapillary. Data for three such tips is shown in Figure S3. Within each data set for a microcapillary, multiple measurements are reported over a range of different sample temperatures from 5 °C to 70 °C. In each case, the calibration fluid is pure water. The calibration constants K_c for these microcapillaries are: $(11,120 \pm 490) \text{ nL}^{-1}$, $(23,140 \pm 270) \text{ nL}^{-1}$, and $(306,300 \pm 6,000) \text{ nL}^{-1}$. The uncertainty of the calibration varies from approximately 1 % to nearly 5 %, depending on the length of data collection time.

The self-consistency of the calibration constant at different temperatures demonstrates that the temperature control is accurate and thermal gradients are negligible. Also, note that thermal expansion of the capillary is negligible, even though K_c changes inversely with volumetric expansion (Eqn 1).

REFERENCES

- ¹G. Ellis, "Control system design guide a practical guide," (Elsevier Academic Press, Amsterdam; Boston, 2004).
- ²J. Kestin, M. Sokolov and W. A. Wakeham, "Viscosity of liquid water in range -8-degrees-c to 150-degrees-c," Journal of Physical and Chemical Reference Data **7** (3), 941-948 (1978).